Customization of RegCM3 Regional Climate Model for Eastern Africa and a Tropical Indian Ocean Domain

NEIL DAVIS, JARED BOWDEN, FREDRICK SEMAZZI, AND LIAN XIE

Department of Marine, Earth, and Atmospheric Sciences, North Carolina State University, Raleigh, North Carolina

BARIŞ ÖNOL

Aeronautics and Astronautics Faculty, Meteorological Engineering, Istanbul Technical University, Maslak, Istanbul, Turkey

(Manuscript received 19 December 2007, in final form 23 January 2009)

ABSTRACT

Rainfall is a driving factor of climate in the tropics and needs to be properly represented within a climate model. This study customizes the precipitation processes over the tropical regions of eastern Africa and the Indian Ocean using the International Centre for Theoretical Physics (ICTP) Regional Climate Model (RegCM3). The convective schemes of Grell with closures Arakawa–Schubert (Grell–AS)/Fritch–Chappel (Grell–FC) and Massachusetts Institute of Technology–Emanuel (MIT–EMAN) were compared to determine the most realistic spatial distribution of rainfall and partitioning of convective/stratiform rainfall when compared to observations from the Tropical Rainfall Measuring Mission (TRMM). Both Grell–AS and Grell–FC underpredicted convective rainfall rates over land, while over the ocean Grell–FC (Grell–AS) over- (under-) estimates convective rainfall. MIT–EMAN provides the most realistic pardoning and spatial distribution of convective rainfall despite the tendency for overestimating total rainfall. MIT–EMAN was used to further customize the subgrid explicit moisture scheme (SUBEX). Sensitivity tests were performed on the gridbox relative humidity threshold for cloudiness (RH_{min}) and the autoconversion scale factor (C_{acs}). An RH_{min} value of 60% (RHmin-60) reduced the amount of total rainfall over five heterogeneous rainfall regions in eastern Africa, with most of the reduction coming from the convective rainfall. Then, C_{acs} sensitivity tests improved upon the total rainfall amounts and convective stratiform partitioning compared to RHmin-60. Based upon all sensitivity simulations performed, the combination of the MIT–EMAN convective scheme, RHmin-60, and halving the model default value (0.4) of C_{acs} provided the most realistic simulation in terms of spatial distribution, convective partition, rainfall totals, and temperature bias when compared to observations.

1. Introduction

The climate of the Greater Horn of Africa (GHA) is difficult to represent on both local and large scales because of complex topography, large inland lakes, contrasts in vegetation, and proximity to the Indian Ocean (Ininda 1998; Anyah and Semazzi 2007; Anyah et al. 2006). One solution to this problem is to adopt the regional climate model (RCM) downscaling approach, which permits the use of higher resolution at significantly reduced computational cost. In previous studies, RCMs have been shown to add value to a climate forecast, both over the GHA and other regions (Sun et al. 1999a,b; Wang et al. 2004; Anyah and Semazzi 2007; Anyah et al. 2006). The additional value brought by RCMs is especially important to precipitation modeling over the GHA, as small changes in land surface characteristics contribute significantly to the diverse spatial patterns of precipitation (Nicholson 1996). Although the higher resolution of surface features is not by itself sufficient to improve the model performance, it is also important to customize the physics of the RCM to the individual domain, while taking advantage of the increased resolution.

Representing precipitation in models continues to be an urgent challenge because of its importance for the generation of climate predictions at scales that are

Corresponding author address: Jared Bowden, Jordan Hall 4144, Box 8208, North Carolina State University Campus, Raleigh, NC 27695.
E-mail: jhbowden@unity.ncsu.edu

DOI: 10.1175/2009JCLI2388.1

relevant to various end user sectors. This challenge can be broken into two parts: model parameterization and model validation. Precipitation parameterizations try to relate the subgrid precipitation processes and the resolved large-scale physics, but this relationship is not fully understood. Validating parameterization schemes is another challenge because of the lack of high-resolution observations, both spatially and temporally, for much of the world (Vaidya 2006). In addition to these problems, there are further challenges for the modeling of precipitation in the tropics. Most schemes are developed and tested in the midlatitudes, where precipitation forcing differs from that of the tropics. Recent studies (Houze 1997; Schumacher and Houze 2003) have given some insight into the forcing and structure of tropical rainfall. By utilizing these insights, parameterizations can be improved to provide a better representation of tropical rainfall.

Sun et al. (1999a,b) performed customization of RegCM2 for a GHA domain, with emphasis on precipitation fields. They found that total rainfall was best represented in RegCM2 using the Grell convective precipitation scheme with the Arakawa–Schubert closure assumption (Grell–AS). Anyah and Semazzi (2007) and Anyah et al. (2006) performed additional simulations over the GHA region, using RegCM3, which included several changes, notably an advanced large-scale precipitation scheme and a more advanced radiation scheme. Anyah et al. (2006) and Anyah and Semazzi (2007) found that with the new changes Grell–AS did not perform as well as Grell using the Fritz–Chappel closure assumption (Grell–FC), and therefore utilized Grell–FC in their simulations. In comparing the RegCM2 and RegCM3 studies we found that, despite the improved physics of RegCM3, the Anyah et al. (2006) and Anyah and Semazzi (2007) studies, which made use of this version, did not perform as well in terms of total precipitation as the results tended to overpredict total precipitation.

While the Sun et al. (1999a,b), Anyah et al. (2006), and Anyah and Semazzi (2007) customizations focused on total precipitation, recent research has shown that the type of precipitation can also have large impacts on climate prediction. This is due to the difference in latent heat release structure from convection and stratiform precipitation. Therefore, deficiencies in the partitioning of convective and stratiform precipitation could generate unrealistic feedbacks on the general circulation of the tropics (Schumacher and Houze 2003). In addition to the importance of rainfall partitioning, we have found that the RegCM3 produces excessively intense rainfall events that occur at daily time scales. These observations lead us not only to examine the monthly and seasonal average total rainfall fields but also to investigate the patterns of convective and large-scale precipitation.

The objective of this study is to improve upon past customizations over the GHA region at the seasonal time scale with particular focus on precipitation fields and to investigate the physical processes responsible for the changes in model output based on the customization. The first model customization is a modified model domain compared to the one we adopted in several previous studies (Fig. 1). This change was motivated by several studies documenting the importance of the Indian Ocean on East African rainfall (Black et al. 2003; Behera et al. 2005). In addition, there is less agreement between the model and observed rainfall patterns over the coastal region of the Indian Ocean. This problem is significant because the coastal region is situated along the pathway of moisture transported from the Indian Ocean into the interior of the GHA region. Since moisture is recycled through evaporation and precipitation as it penetrates the continental landmass, any deficiencies in the coastal rainfall could have adverse negative effects on model performance over the GHA region. Anyah et al. (2006) demonstrated that, for the Lake Victoria Basin, the eastern boundary contributes approximately 80% of the large-scale moisture that eventually falls as rain over the lake basin. Also, Bowden (2004) suggested that warm pool eddies in the Indian Ocean along the GHA coast can have large impacts on intraseasonal precipitation. The modified model domain therefore extends further into the Indian Ocean than in Sun et al. (1999a,b), Anyah et al. (2006), and Anyah and Semazzi (2007), as the domain used in previous studies may not have included enough of the Indian Ocean to detail these processes.

Additional customizations were made to RegCM3, focusing on the precipitation parameterizations. This involved testing the various convective parameterization schemes provided in RegCM3 and performing sensitivity tests on the adjustable parameters provided by the subgrid explicit moisture (SUBEX) large-scale precipitation scheme. While previously Sun et al. (1999a,b), Anyah et al. (2006), and Anyah and Semazzi (2007) tested the choices of convective parameterizations offered in RegCM at those times, a new parameterization scheme, Massachusetts Institute of Technology–Emanuel (MIT–EMAN) has been added to RegCM3 and has not been tested for this region. MIT–EMAN has been optimized and evaluated specifically for tropical convection, unlike either Grell–FC or Grell–AS. In addition to evaluating the convective parameterizations, we also wanted to test the impact of several parameters in the SUBEX large-scale precipitation scheme for a tropical environment. The SUBEX scheme has been shown to

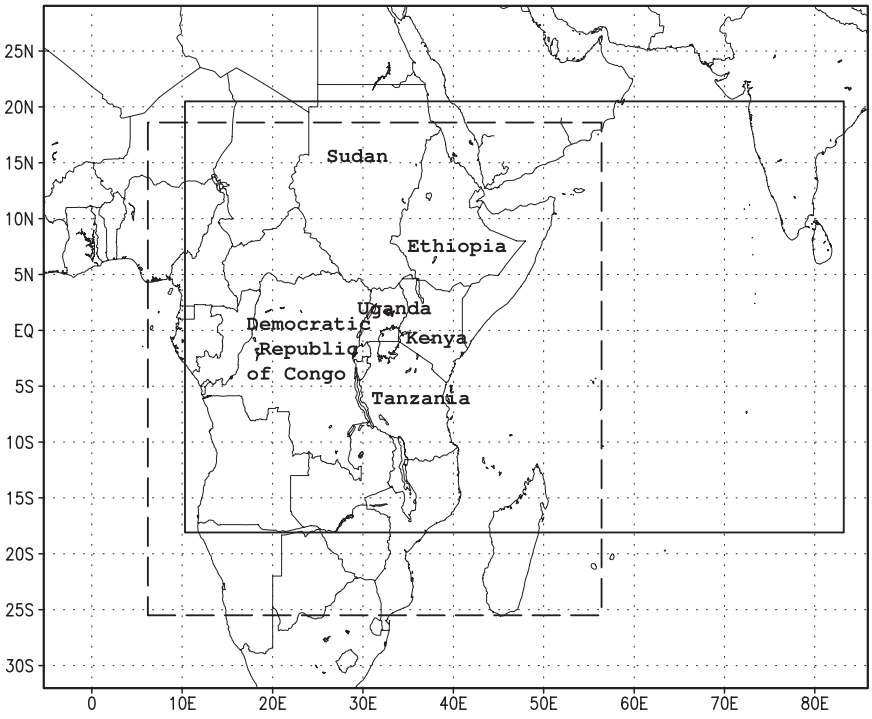

FIG. 1. RegCM domain comparison: previous studies African domain (dashed); current study Indian Ocean domain (solid).

greatly improve precipitation over the midlatitudes (Pal et al. 2000) but has not been thoroughly investigated for the tropics.

As in previous studies, this study focuses on the short rains season [October, November, December (OND)]; however, instead of basing the validation on one normal year (1988) as a proxy to climatology (Ininda 1994; Sun et al. 1999a,b), we use a recent 3-yr climatology to emphasize the robustness of the model customization and investigation of the modeled moist processes. The years chosen (2000, 2001, 2002) allow us to take advantage of Tropical Rainfall Measuring Mission (TRMM) rainfall and Climatic Research Unit (CRU) temperature observations for validation.

2 Model description

a. RegCM3 base

The International Centre for Theoretical Physics (ICTP) Regional Climate Model system version 3 (RegCM3) used in this study is an updated version of the model previously customized for East Africa by Sun et al. (1999a,b). RegCM3 is a hydrostatic model based on the fifth-generation Pennsylvania State University–National Center for Atmospheric Research Mesoscale Model (MM5). It utilizes the National Center for Atmospheric Research (NCAR) Community Climate Model version 3 (CCM3) radiative transfer package for parameterizing radiation. For parameterizing the land surface interactions the Biosphere–Atmosphere Transfer Scheme (BATS 1e; Dickinson et al. 1993) is used. To drive BATS an explicit planetary boundary layer (PBL) scheme is required and the RegCM3 makes use of a nonlocal PBL scheme developed by Holtslag et al. (1990). The large-scale precipitation scheme and several convective parameterization scheme options in the standard version of the model are briefly discussed below. For more detailed descriptions of RegCM3 see Giorgi et al. (1993a,b), Giorgi and Mearns (1999), and Pal et al. (2007).

b. Boundary conditions and other specifications/customizations

RegCM3 requires initial and boundary conditions for wind, temperature, surface pressure, and water vapor, as well as an oceanic surface forcing. For the atmospheric variables, we use National Centers for Environmental Prediction (NCEP)–NCAR reanalysis product version 2 (NNRP2; Kistler et al. 2001) and, for the oceanic surface forcing, weekly updated National Oceanic and Atmospheric Administration (NOAA) Optimum Interpolation Sea Surface Temperature (OISST;

Reynolds and Smith 1994). RegCM3 has two options for the ocean flux. This study adopts the BATS ocean flux scheme, which uses standard Monin–Obukhov similarity relations with a constant roughness length. Soil moisture and temperature were initialized using the standard RegCM3 lookup tables. The model is run using 18 vertical levels with a model top pressure of 50 hPa and 60-km grid spacing. The first month of each 4-month run, starting from the beginning of September, is discarded for spinup of the atmosphere; however, this may not be sufficient time to spin up longer memory processes such as soil moisture.

c. Convective schemes

RegCM3 has four options for representing cumulus convection. These four options are Kuo (Anthes 1977); Grell (Grell 1993), which can use either the Arakawa–Schubert (Grell–AS; Arakawa and Schubert 1974) or the Fritsch–Chappell (Grell–FC; Fritsch and Chappell 1980) closure schemes; and Massachusetts Institute of Technology–Emanuel (MIT–EMAN; Emanuel 1991; Emanuel and Zivkovic-Rothman 1999) cumulus cloud schemes. The Kuo scheme was not tested in this study because the previous study of Sun et al. (1999a) found it to perform poorly for this region.

1) GRELL CUMULUS CLOUD SCHEME

The Grell (1993) scheme is designed to avoid first-order sources of error. The clouds are represented by two steady-state circulations, an updraft and a downdraft. Direct mixing between the cloud air and environmental air is allowed only through the base and top of the cloud. This results in a constant cloud mass flux in the updraft (m_b) and downdraft (m_o) with height. The originating levels of the updraft and downdraft are given by the levels of maximum and minimum ambient moist static energy, respectively. Activation of the scheme occurs when a parcel attains moist convection. Condensation within the updraft occurs as a saturated air parcel is lifted. The originating mass flux of the downdraft is a function of the updraft mass flux. The parameter β relates the updraft to the downdraft, dependent on wind shear, and represents the reevaporation of convective condensate in the downdraft, where $1 - \beta$ is the precipitation efficiency. Precipitation is given by

$$P = I1 * m_b(1 - \beta), \tag{1}$$

where $I1$ is the normalized updraft condensate (Grell 1993; Giorgi and Shields 1999).

This study uses two closure assumptions for calculating m_b. In the Arakawa and Schubert (1974) (Grell–AS) closure, the updraft mass flux is determined under the assumption that the cloud-work function is in a quasi-equilibrium state. The mass flux in the updraft is therefore given by

$$m_b = \frac{\mathrm{ABE}'' - \mathrm{ABE}}{\mathrm{NA(DT)}}, \tag{2}$$

where ABE is the available buoyant energy for convection, ABE″ is the available buoyant energy generated from large-scale motions during the model time step (DT), and NA is the rate of change of ABE per unit m_b. The ABE″ is computed using the atmospheric variables at the current time step plus the tendencies due to dry adiabatic adjustment and heat–moisture advection (Giorgi et al. 1993b). In general, Eq. (2) represents the removal of buoyant energy generated from large-scale motions by convective clouds in a single model time step Giorgi and Shields (1999).

Grell–FC is also a stability-based closure assumption, relying on the presence of available buoyant energy. It assumes that the ABE is removed by convection over a given time scale, shown as follows:

$$m_b = \frac{\mathrm{ABE}}{\mathrm{NA}\tau} \tag{3}$$

where τ is the ABE removal time scale (Giorgi et al. 1993b). For this study, τ is 30 min and is comparable to previous values of 20 and 40 min tested by Giorgi et al. (1993b).

These two assumptions differ in that Grell–AS relates convection to large-scale buoyant energy production, while the Grell–FC relates convection to the degree of instability. However, both closures may be less valid in the tropics where there is no strong relationship between convective precipitation and ABE (Cotton and Anthes 1989).

2) MIT–EMAN CUMULUS CLOUD SCHEME

The most recent cumulus scheme added to RegCM3 is MIT–EMAN (Emanuel 1991; Emanuel and Zivkovic-Rothman 1999). This scheme does not make the assumption of many traditional convective schemes where convective clouds are modeled as entraining plumes. Instead this scheme assumes the mixing in clouds is highly episodic and inhomogeneous. The convective fluxes are represented using an idealized model of subcloud-scale updrafts and downdrafts. Convection is assumed to occur when the level of neutral buoyancy is at a higher altitude than the level of the cloud base. Air is lifted from each subcloud layer to an arbitrary level between itself and the level of neutral buoyancy where a fraction of the condensed water is converted to precipitation. The cloudy air is mixed with its environment

at the arbitrary level and ascends or descends to its new level of neutral buoyancy. The entrainment and detrainment rates are functions of the vertical gradients of buoyancy in the clouds. The net upward mass flux of undiluted air through the cloud base is determined using the subcloud layer quasi-equilibrium theory. The concept is that the time for the surface fluxes and radiative cooling to destabilize the subcloud layer is relatively short (Emanuel and Zivkovic-Rothman 1999).

MIT–EMAN offers several advantages to other convective schemes available in RegCM3. First, it includes an autoconversion threshold, which is temperature dependent; therefore, ice processes are crudely accounted for (Emanuel and Zivkovic-Rothman 1999). Also, the precipitation is added to a single hydrostatic, unsaturated downdraft, which transports heat and water. In addition to these advancements, this scheme has been optimized and evaluated for tropical convection, which is an important consideration for this study.

d. Subgrid explicit moisture scheme

SUBEX (Pal et al. 2000) was developed to treat nonconvective cloud and precipitation processes in RegCM replacing the older simple explicit moisture (SIMEX) scheme. SUBEX calculates the autoconversion of cloud water to rainwater, accretion, evaporation, and cloud fraction at each grid point. The cloud fraction (CF) equation adopted by Pal et al. (2000) is based on Sundqvist (1988) and may be stated as follows:

$$\mathrm{CF} = 1 - \sqrt{1 - \frac{\mathrm{RH} - \mathrm{RH}_{\min}}{\mathrm{RH}_{\max} - \mathrm{RH}_{\min}}}, \tag{4}$$

where RH is the gridpoint relative humidity, $\mathrm{RH}_{\min}$ is the relative humidity threshold where clouds start to form, and $\mathrm{RH}_{\max}$ (101% in all studies) is the relative humidity where CF reaches one. The cloud fraction equation allows SUBEX to treat part of each grid box as cloudy and precipitating, while the rest of the grid box is cloud free. This was one of the major improvements over the previous schemes. In RegCM3, $\mathrm{RH}_{\min}$ is an adjustable parameter that can be defined separately for land and ocean.

The other major change brought by the SUBEX scheme was a change to the autoconversion threshold (Q_c^{th}). The settings for Q_c^{th} in SUBEX were based on results from Gultepe and Isaac (1997), who utilized cloud liquid water and temperature data from aircraft observations to determine numerical relationships between the two parameters. Pal et al. (2000) relied upon one of the cloud liquid water–temperature relationships to determine Q_c^{th} described below:

$$Q_c^{\mathrm{th}} = C_{\mathrm{acs}} 10^{-0.49+0.013T} 0.001, \tag{5}$$

where C_{acs} is the autoconversion scale factor, and T is the temperature in degrees Celsius. The Q_c^{th} was then used to generate the amount of cloud water converted to rain, autoconverted, by SUBEX. The updated autoconversion calculation used in SUBEX showed improvement over the previous scheme in the sensitivity tests completed by Pal et al. (2000) over the United States; however, we found SUBEX was producing too much stratiform precipitation over our tropical domain, discussed in section 5c. Since Pal et al. (2000) noted that SUBEX-generated precipitation was highly sensitive to the Q_c^{th} parameter, we investigated the relationship derived by Gultepe and Isaac (1997) by adjusting C_{acs}, which is an adjustable parameter in RegCM3. For a full description of SUBEX and its incorporation in RegCM3, see Pal et al. (2000).

e. Relationship between convective scheme and SUBEX

In RegCM3, both the convective and SUBEX schemes work on subgrid scales; however, their approaches are different. The convective schemes try to diagnose if convection will occur in portions of the grid. This allows them to emulate updrafts in the atmosphere and form precipitation through those updrafts. The large-scale precipitation scheme SUBEX does not emulate updrafts, but instead processes the moisture that is already aloft in the atmosphere. In this process it forms clouds and precipitation if critical thresholds of moisture are surpassed). In RegCM3 the convective scheme is called before the SUBEX scheme. This implies that some SUBEX precipitation could be generated by moisture moved aloft by the convection that moves moisture aloft but that the convective scheme itself does not rain out. For this study the separation of convective and stratiform rain was dependent on which scheme generated the rainfall.

3. Validation data

a. TRMM precipitation

The TRMM satellite platform provides multiple rainfall products from each of its various rainfall sensors. We use the TRMM 3A-12 version 6. TRMM product 3A-12 6 uses the 2A12 TRMM Microwave Imager (TMI) retrieval algorithm to partition rainfall into convective and stratiform categories (Kummerow et al. 2001). We chose the TMI option over the TRMM Precipitation Radar (PR) estimates because the PR swath width is around one-third of the TMI. The additional coverage of the TMI is recommended for climate

studies. In addition, Robertson et al. (2003) compared discrepancies in tropical mean rainfall between PR and TMI. They found that the variability in the PR path-integrated attenuation closely matches the variability in the TMI rain estimates, suggesting that uncertainties in the assumed drop size distribution and the associated reflectivity–rainfall relationships inherent in single radar methods is a serious issue for climate studies. TRMM 3A-12 also allows us to compare the inherent strengths and weaknesses of the model convective and large-scale precipitation, in addition to estimated total rainfall.

b. CRU TS 2.1: Surface temperature

For temperature observations over land we used the Climate Research Unit's CRU TS 2.1 dataset (Mitchell and Jones 2005). CRU TS 2.1 is a monthly gridded climatology of station data for the period 1901–2002. To construct a global dataset, station data were collected from several sources. The data were then corrected, discarded, or combined using an automated process that checks for many possible problems in the original data. To ensure that all data were tested an iterative process was used. After the correction, a reference series of climatological normals was calculated and used in the calculation of station anomalies. These anomalies were then interpolated to a 0.5° grid covering the global land surface and anomalies added back to the climatological normals to produce gridded temperatures. The temperature portion of the data contains estimates for 80%–100% of the land surface. For a full description of the techniques used in compiling this dataset see Mitchell and Jones (2005).

c. NCEP–DOE reanalysis 2

To conduct observational comparisons with the model for 850-hPa circulation and 2-m over-ocean temperatures we used the NCEP–Department of Energy (DOE) reanalysis 2 dataset (Kistler et al. 2001) since direct observations are very sparse. This dataset is an updated version of the NCEP–NCAR 50-Year Reanalysis. It has a 2.5° latitude and longitude resolution. The reanalysis system uses a model that assimilates the observations using the three-dimensional variational data assimilation (3DVAR) scheme. This setup generates 3 types of variables: 1) type a, which are mostly influenced by observations; 2) type b, which are influenced by both observations and the model; and 3) type c, which are almost completely generated by the model. For the tropics, both the 2-m over-ocean temperature and circulation are considered type b variables. A full description of the NCEP–NCAR reanalysis can be found in Kistler et al. (2001).

4. Design of model experiments

a. Convective schemes experiments

Three model runs were performed to compare the convective schemes: two for the Grell scheme, one for each closure method (Grell–AS and Grell–FC), and one for MIT–EMAN. All runs used model defaults for the adjustable parameters in each scheme. The RegCM3 model results for 850-hPa circulation, 2-m temperature, and partitioned/total precipitation will be compared with the observed data (see section 3). To assess the performance of each scheme, area averages of convective and stratiform rainfall are computed for different regions of GHA. The previous model customization of Sun et al. (1999a) used similar geographic rainfall regions based on Nicholson et al. (1988). However, their regions were based on the annual rainfall climatology, rather than the OND seasonal rainfall climatology, and did not include a large portion of the GHA region. Indeje et al. (2000) used cluster analysis and found eight homogeneous climate zones over East Africa, but the homogeneous zones did not include areas north of Kenya or west of Uganda/Tanzania. Figure 2 shows the five new geographical regions utilized in this study based on a 1961–90 OND seasonal rainfall climatology from the CRU dataset. We name each region using the name of the country that accounts for the largest percentage of area for that particular zoning type. The regions are the 1) semiarid region of northern Ethiopia and Sudan (SUD), 2) wetter mountainous region of Ethiopia (Ethiopian highlands; EH), 3) tropical rain forest region (Congo; CO), 4) Lake Victoria and Kenya highlands (KE), and 5) Tanzania (TA). Seasonally averaged model biases will also be computed for partitioned/total precipitation and temperature. The precipitation model bias is computed using the method found in Giorgi and Shields (1999). This provides bias as a percentage of the observed value. We also compare the convective percentage—total rain divided by convective rain—of each scheme with observations. Finally, we calculated equivalent potential temperature

$$\theta_e = \theta e^{Lw_s/C_pT}, \tag{6}$$

where θ is the potential temperature, L is the latent heat of vaporization, w_s is the saturation mixing ratio, c_p is specific heat at constant pressure, and T is temperature. Here θ_e was calculated using the gridbox average values of dewpoint, relative humidity, surface pressure, temperature, and θ at the onset of convection for each of the 18 vertical levels for 2001. We were then able to create an average vertical profile for the convective events generated by each scheme. A convective event was defined as

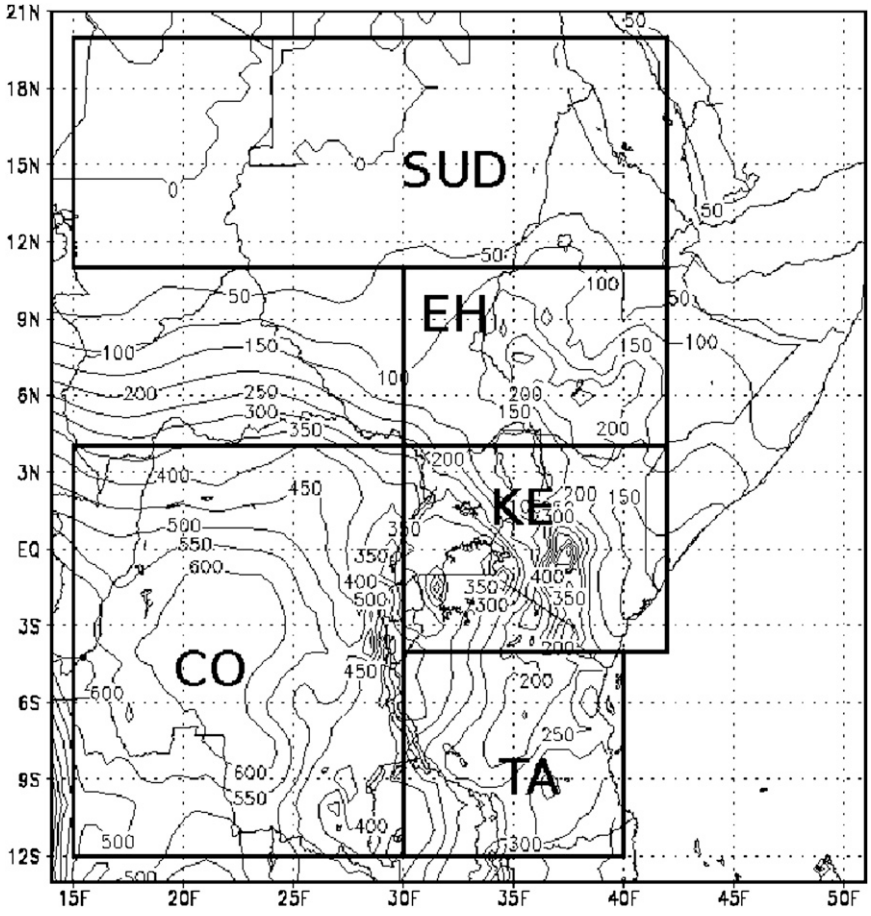

FIG. 2. Five regions used for statistical analysis. Semiarid region (SUD), Ethiopian highlands (EH), tropical rain forest (CO), Kenyan highlands and Lake Victoria Basin (KE), and Tanzania (TA). Isolines show 1961–90 OND climatological precipitation (mm yr^{-1}) based on CRU observations.

the first output time period where rainfall was greater than 0.1 mm h^{-1}, until rainfall fell below that threshold at each grid cell. Table 1 shows that for each scheme there were more than 300 000 events. Although only 1 yr of data was used in this analysis we feel that it provides an accurate average vertical profile because of this large number of events. In addition, we had to perform quality control on a small amount of modeled data shown in Table 1 as some of the values were well above the natural threshold of θ_e. The chosen threshold eliminated 451 events from Grell–FC, which is more than double that of Grell–AS and tenfold that of MIT–EMAN. Using these techniques we are able to show which schemes perform well for the various tests in addition to which scheme provides the best total rainfall representation.

b. SUBEX experiments

This category of experiments focuses on the large-scale SUBEX cloud and precipitation scheme. While comparing the convective schemes, we found that stratiform rain was overpredicted regardless of the scheme. Since SUBEX has been validated for the midlatitudes, we looked for calculations and, in particular, constants used in the scheme that would be most affected by a tropical environment. The two calculations we examined in detail were the autoconversion of cloud water to rainwater and the amount of gridbox relative humidity needed for cloud formation (RH_{min}). Pal et al. (2000) has documented typical values for RH_{min} in the model as being between 60% and 100%. The default values in the model are 80% over land and 90% over the ocean.

TABLE 1. Number of convective events used to calculate average θ_e profiles.

	Grell–AS	Grell–FC	MIT–EMAN
Total No. of convective events	372 479	335 935	351 884
No. deleted in quality control	171	451	45

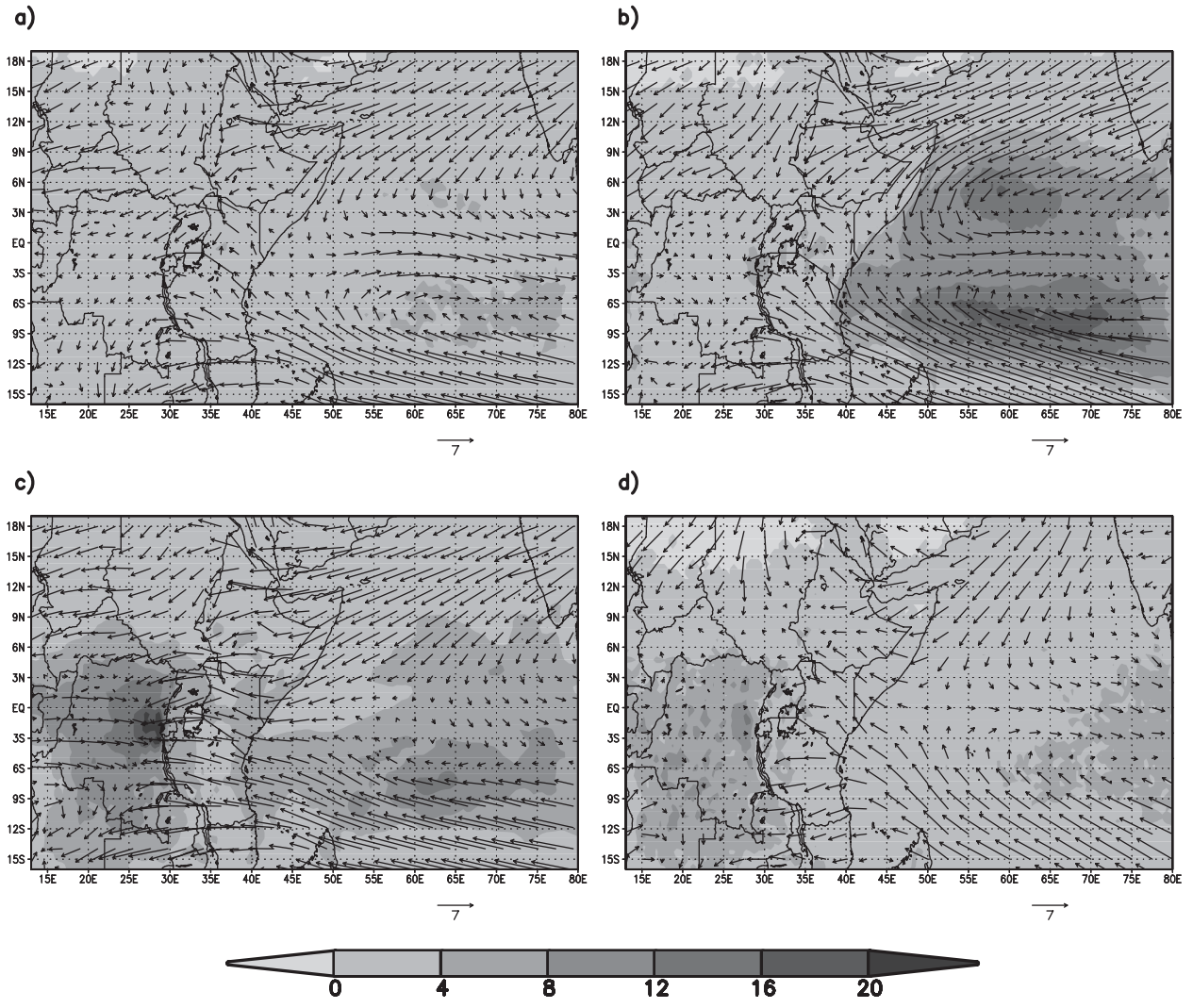

FIG. 3. Three-yr climatological OND convective rainfall (mm day^{-1}) and 850-hPa circulation (m s^{-1}) for (a) Grell–AS, (b) Grell–FC, (c) MIT–EMAN, and (d) TRMM (rainfall) and NCEP winds.

To test the sensitivity of the model performance on this important parameter we relied on previous studies that performed sensitivity testing on the RH_{min} parameter using schemes similar to SUBEX (Zhao et al. 1997; Del Genio et al. 1996).

Zhao et al. (1997) implemented a SUBEX-type scheme to the NCEP Eta Model. In the study RH_{min} was set to 75% over land and 85% over the ocean, similar to the RegCM3 default. The study explains that higher RH_{min} values are used over the ocean to avoid excessive condensation, which could occur in a climate with increased surface moisture. Since a large portion of our region is located in the moist tropics, and RegCM3 uses an RH_{min} of 90% as the default for the ocean, we chose to test the model with a 90% RH_{min} (RHmin-90) over land.

Our second test is based on the work of Del Genio et al. (1996). This study created a SUBEX-type scheme for GCMs and found an RH_{min} of 60% to perform well, which is the value used in our second SUBEX test (RHmin-60). While 60% was the preferred value, they found that the GCM still overpredicted rainfall for regions of high relative humidity. Despite this noted problem, we chose this value as an important sensitivity test since the GCM study includes tropical regions, unlike Zhao et al. (1997) or Pal et al. (2000). The results of these studies were compared using the same approach as in the convective scheme experiments (section 4a).

Additional sensitivity tests were performed on the autoconversion scale factor C_{acs}. The autoconversion threshold is based off an empirical function by Gultepe and Isaac (1997) that was determined from observations

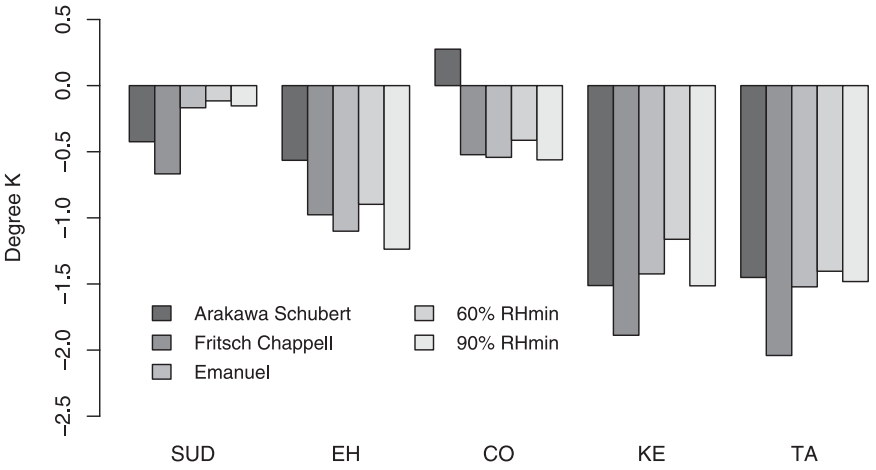

FIG. 4. Temperature bias (K) across all simulations for each of the five heterogeneous rainfall regions of East Africa.

obtained in Canadian and Russian field studies. Gultepe and Isaac (1997) found a maximum liquid water content (LWC) of 26 g m^{-3} in those field studies; however, Iacobellis and Somerville (2000) found that, during the Tropical Ocean and Global Atmosphere Coupled Ocean–Atmosphere Response Experiment (TOGA COARE) study, over 70% of the warm liquid water clouds had an LWC of above 0.25 g m^{-3}. For sensitivity

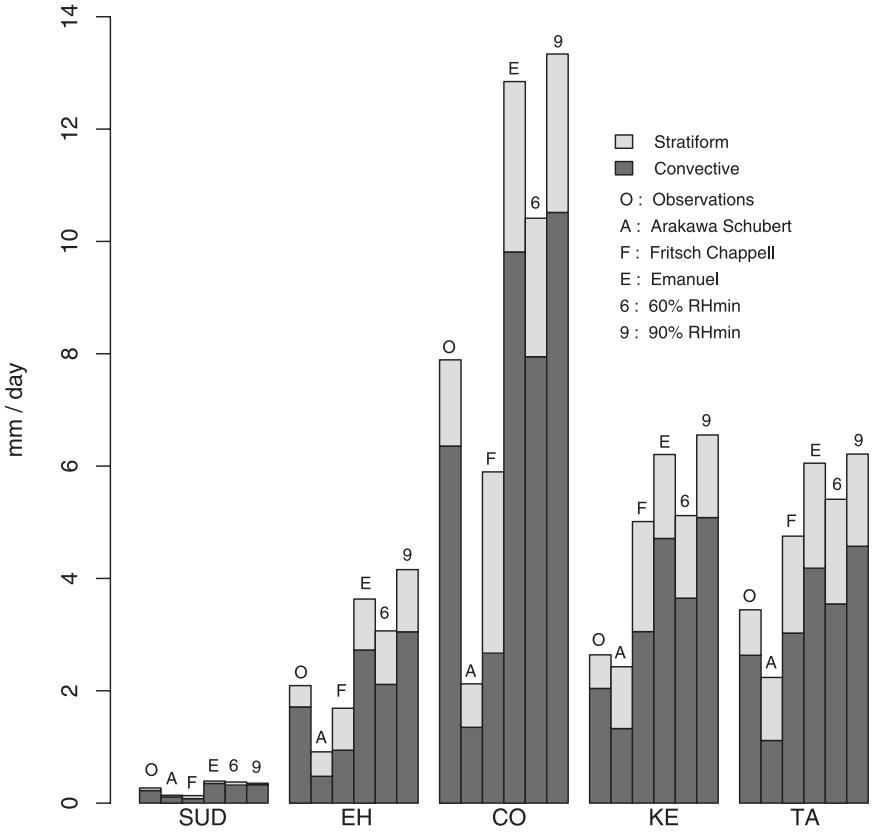

FIG. 5. Observed and simulated rainfall totals (mm day^{-1}) partitioned into convective and stratiform rainfall across all simulations for each of the 5 heterogeneous rainfall regions of East Africa.

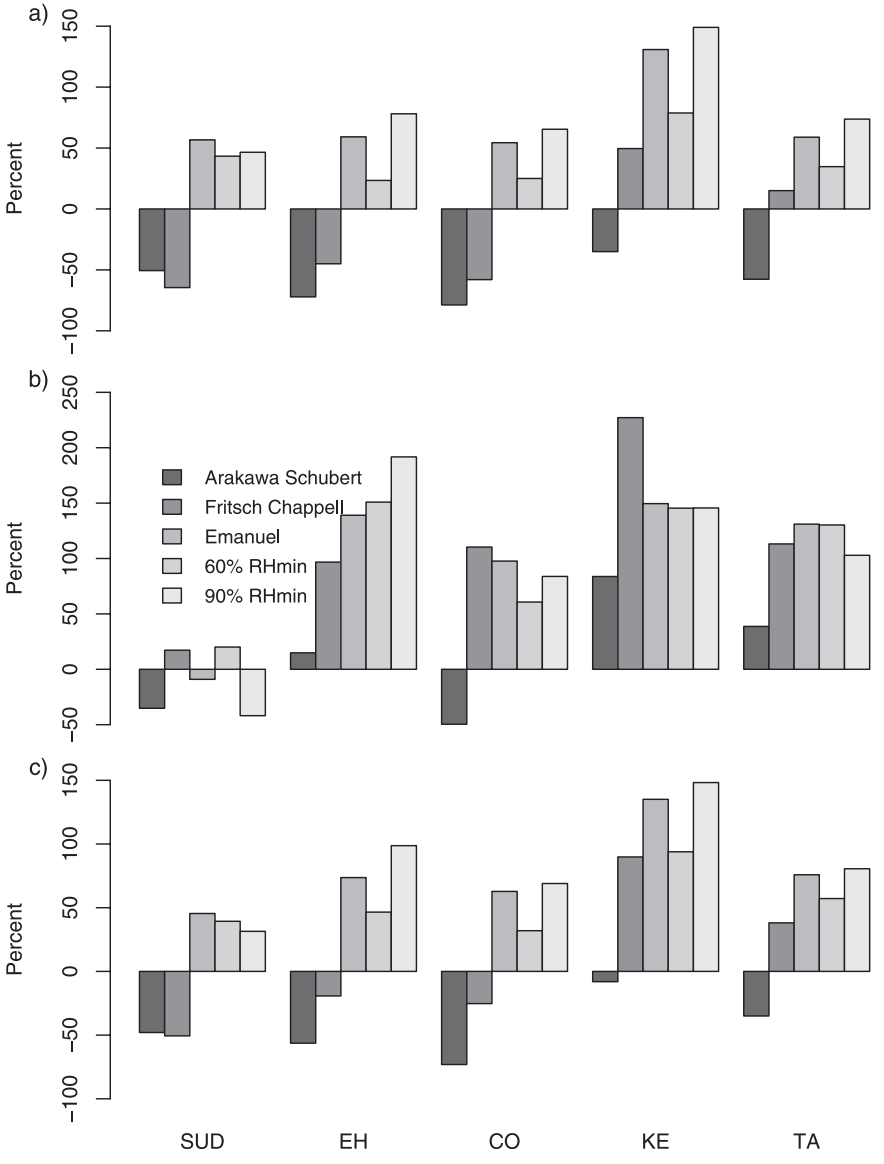

FIG. 6. Percent rainfall bias, model vs TRMM observations, for (a) convective, (b) stratiform, and (c) total rainfall.

purposes, the C_{acs} was doubled (C_{acs}-double) and halved (C_{acs}-half) from its default value of 0.4. In C_{acs}-double the atmosphere is able to hold more cloud liquid water; therefore, less cloud liquid water is converted to rain.

5. Results

a. Convective schemes—Qualitative comparison

A multiyear climatological average of the convective schemes is tested over the Indian Ocean domain during the OND season. The discussions will identify strengths and weaknesses of each scheme and closure.

1) GRELL–AS SCHEME

Figure 3 is a plot of the average convective precipitation for each scheme compared with average TRMM convective precipitation. The 850-hPa circulation is included to illustrate the sensitivity of the simulated large-scale flow to the choice of convective scheme.

There is little to no convective rainfall for Grell–AS over land. More interestingly, there is little rainfall, less than 2 mm day^{-1}, over the Congo tropical rain forest. In contrast, observed TRMM rain rates demonstrate convective rainfall rates of 9–12 mm day^{-1} over the Congo. Similarly, Schumacher and Houze (2003) examined stratiform and convective rain rates for the tropics

and their results were consistent with the dominance of convective precipitation over the Congo tropical rain forest based on comparison with TRMM data. Giorgi and Shields (1999) noted that the Grell–AS closure tends to minimize convection because it forces dissipation of large-scale buoyant energy within a single model time step. This limited convective activity over land has little feedback on the large-scale circulation. Therefore, the RegCM3 circulation closely resembles the NCEP reanalysis circulation, which was used for the initial and boundary conditions. Over the Indian Ocean, convective rain rates increase and are closer to observed values. This is not consistent with the expectation that convective activity on average tends to decrease over the oceans relative to land. Oceanic environments are favorable for stratiform precipitation via a warm, moist boundary layer with a small diurnal temperature range and/or the near-moist adiabatic stratification of the free atmosphere (Schumacher and Houze 2003). However, anomalous events, such as El Niño and positive Indian Ocean dipole events, can favor intense convective rainfall.

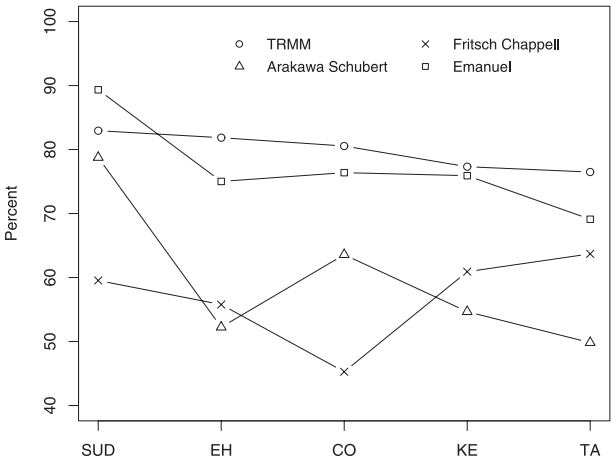

FIG. 7. Area-averaged convective percentage for Grell–AS, Grell–FC, and MIT–EMAN simulations and TRMM observations for each of the five heterogeneous rainfall regions of East Africa.

2) GRELL–FC SCHEME

Grell–FC produces more convective precipitation over both the land and ocean than Grell–AS. This is consistent with previous experiments of Giorgi et al. (1993a). Grell–FC also produces better convective rainfall amounts over land in comparison to Grell–AS. The convective coverage of rainfall increases over the Congo tropical rain forest, coastal East Africa, southern Kenya, and Tanzania. There is little convection over the Ethiopian highlands. In comparison with TRMM observations over the Congo tropical rain forest, the convective precipitation is sparse and maximum rain rates are too small, 3–6 mm day^{-1} compared to 9–12 mm day^{-1}. Furthermore TRMM has little convective precipitation over Kenya/Tanzania but greater convective activity over the Ethiopian highlands, both of which are poorly represented in the model. Over the Indian Ocean the convective precipitation is organized in a double band pattern, centered on 5°N and 7°S. Both bands are very intense with maximum rain rates around 20 mm day^{-1} for the entire season. TRMM does show a weak double band feature around similar latitudes, but the intensity, 3–6 mm day^{-1}, and horizontal extent of the precipitation is less than in the Grell–FC experiment. The convective feedback generates an unrealistic cyclonic flow centered on the intense rainfall bands. Again, over the ocean convective rain rates are larger than over land.

3) MIT–EMAN SCHEME

The most notable change between MIT–EMAN and either Grell–AS or Grell–FC occurs over the Congo tropical rain forest. The spatial coverage of modeled convective activity is continuous from 15°S to 5°N and 15° to 30°E. The model also captures the observed maximum rainfall feature centered at 15°S, 28°E. However, the modeled convective rainfall rates are larger than observed throughout most of the Congo tropical rain forest. The overestimation in convection is partly explained by examining the circulation. The modeled westerlies over the Congo tropical rain forest originate from the Atlantic Ocean favoring an increase in low-level moisture, increasing the instability. MIT–EMAN also increases convective precipitation coverage over the Ethiopian highlands. The convection over the Ethiopian highlands is more widespread in the model, but has similar rain rates of 3–6 mm day^{-1}. Similar to Grell–FC, the convective precipitation increases over East Africa when using MIT–EMAN. As for the Indian Ocean, the modeled convection extends from 10°S to 10°N, with exceptions along some portions of the Somalia coast. MIT–EMAN produces a similar double precipitation band as in the case of the Grell–AS and Grell–FC and has a similar problem of overestimating the longitudinal extent of the precipitation bands. The most intense convection is centered near 7°S, 63°E with rain rates between 15 and 18 mm day^{-1}. These rain rates are nearly twice the observed maximum convective rain rates of 6–9 mm day^{-1}. The northeasterly and southeasterly winds are more intense than observed along the equatorial region. The low-level convergence over the western equatorial Indian Ocean is opposite to the observed field partially explaining the overestimation and longitudinal extent of the convective precipitation. While the model overestimates oceanic precipitation, it

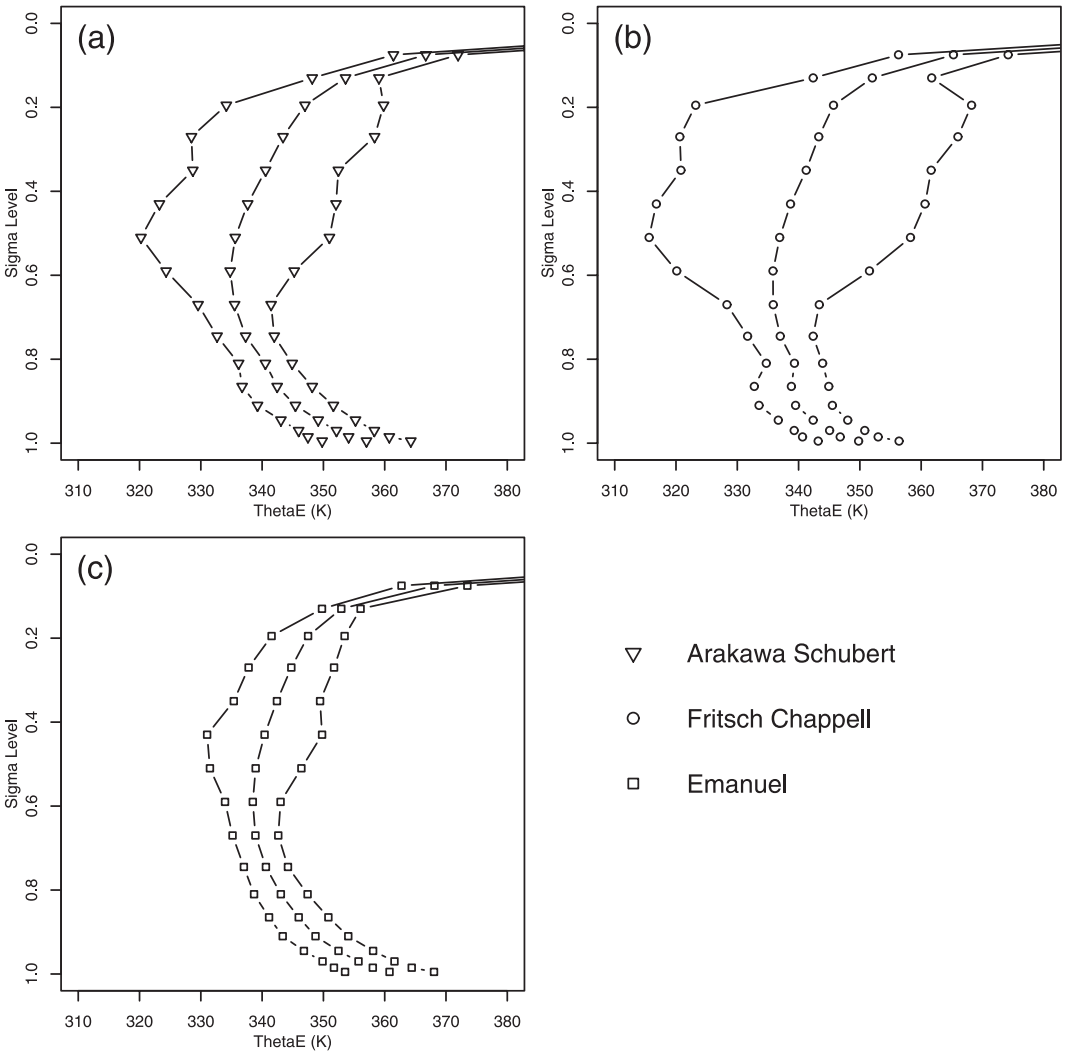

FIG. 8. Equivalent potential temperature vertical profiles in a convective environment for (a) Grell–AS, (b) Grell–FC, and (c) MIT–EMAN. Centerline is the mean across all convective events, with the outside line being ± one standard deviation from the mean.

does generate more convective rainfall over land, in agreement with observations.

b. Convective schemes–quantitative comparison

RegCM3 tends to have a cold temperature bias at 2 m for all convective schemes and regions, with only one exception, over the Congo for the Grell–AS scheme (Fig. 4). As previously shown for this scheme, there is little convective rainfall over the Congo favoring increased surface sensible heating and a positive temperature bias. Each region exhibits a similar temperature bias response regardless of the scheme. The largest bias in each scheme is over Kenya and Tanzania, with Grell–FC exhibiting the worst bias for those regions, near −2.0 K. On average for all the regions Grell–AS, Grell–FC, and MIT–EMAN have −0.7, −1.2, and −1.0 K temperature biases, respectively. These small changes in temperature bias show that, although the precipitation field is greatly affected by the choice of convective parameterization, the model temperature is influenced predominately by other factors. In addition we found that such small differences in temperature bias are not very helpful in deciphering the best scheme available for this study.

Figure 5 is a comparison plot of convective and total precipitation for the five geographic regions. The model underestimates total precipitation throughout the area average regions for Grell–AS and overestimates for MIT–EMAN. Grell–FC overestimates rainfall in KE and TA and underestimates elsewhere.

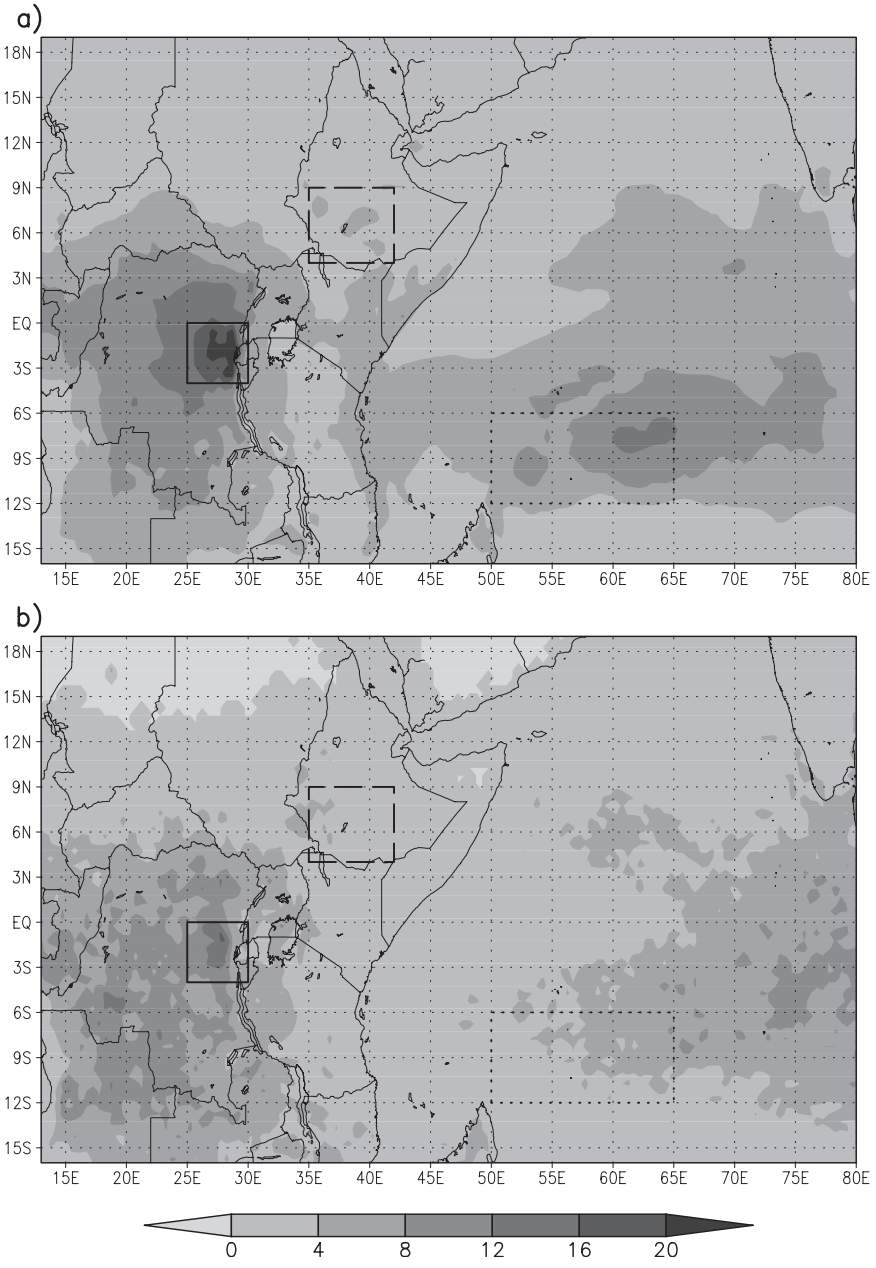

FIG. 9. (a) MIT–EMAN total rainfall and (b) TRMM observed rainfall (mm day^{-1}) emphasizing problematic regions for the simulation: southwest Ethiopia (dashed), eastern tropical rain forest (solid), and Indian Ocean (dotted).

Figure 6a quantifies the percent bias for convective rainfall. The convective bias for Grell–AS is negative for each region and largest over CO, with a 79% decrease. Over all regions, Grell–AS has an average negative bias of 59%. As mentioned above, the convective bias for Grell–FC is regionally dependent. The regions SUD, EH, and CO each have a negative bias with an average of 56%. The coastal regions of KE and TA have a weaker average positive bias of 32%, with the largest comparatively being only 50% over KE. The convective bias in MIT–EMAN is positive throughout all the regions and on average 72%. The largest bias, similar to Grell–FC, is located over KE where the bias is more than double that of the other regions. The large bias over KE for both schemes depicts that the model tends to have a problem modeling convection over this region. The problem may be related to the elevated terrain. As noted in Giorgi and Shields (1999)

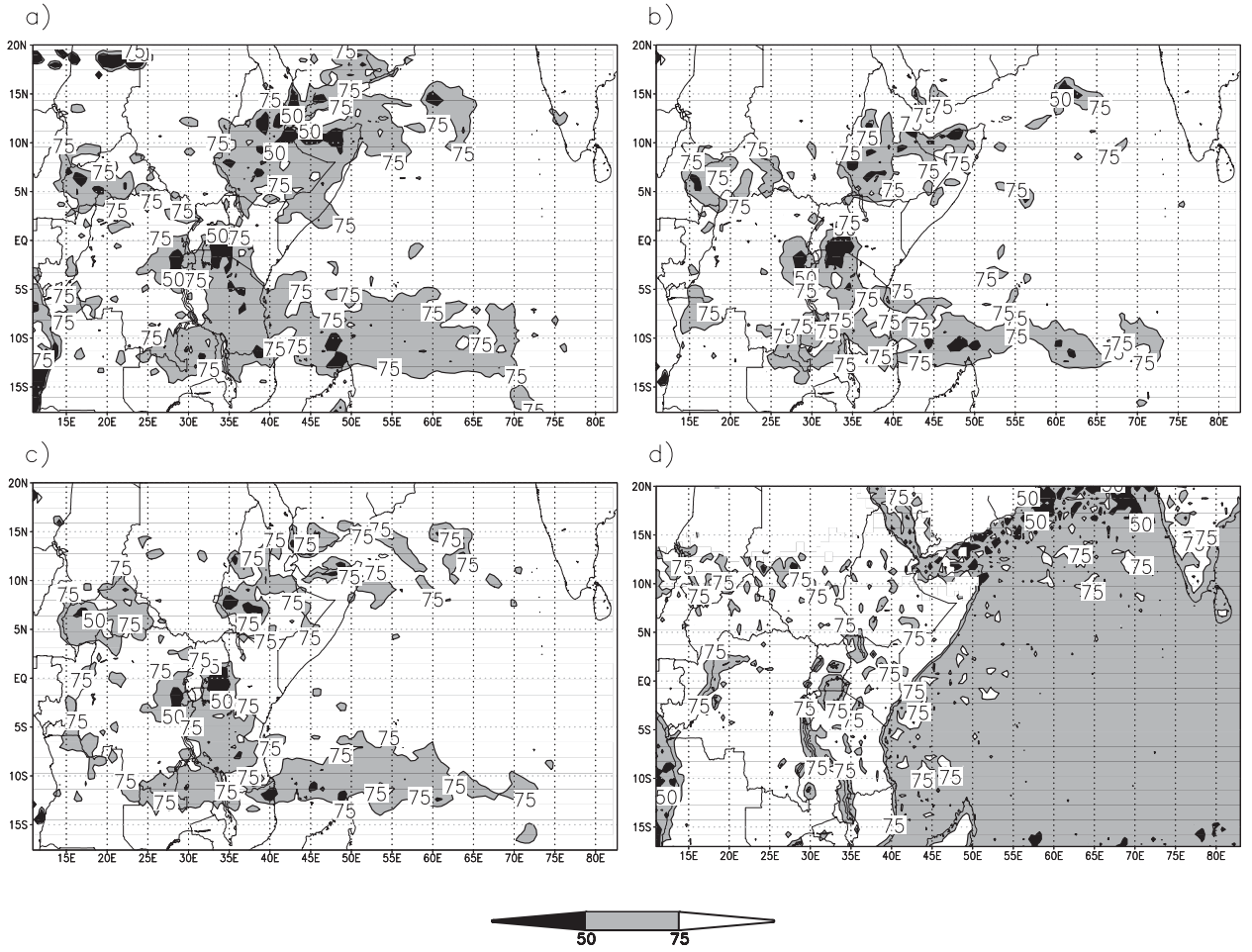

FIG. 10. Convective percentage for (a) RHmin-60, (b) RHmin-90, (c) MIT–EMAN, and (d) TRMM.

in a previous version of RegCM, model performance declined in the higher-terrain area of the western United States.

Figure 6b quantifies the percent bias for stratiform rainfall. The only negative stratiform biases occur for Grell–AS over the SUD and CO regions and MIT–EMAN over the SUD region. The results suggest that RegCM3 typically overestimates stratiform rainfall over the GHA. Grell–FC has the worst overall stratiform bias, with a positive bias on average of 113% that exceeds 220% over KE. Similarly, Grell–AS and MIT–EMAN perform the worst over KE.

Figure 6c quantifies the percent bias for total rainfall. The sign of the total rainfall bias for each scheme follows the sign of the convective bias. This is not surprising since the convective rain rates are almost always larger than those of stratiform. Since the stratiform bias tends to be positive for all regions and schemes, it decreases (increases) the total rainfall bias for negatively (positively) biased regions.

Figure 7 demonstrates the accuracy of model rainfall partitioning by examining the model percent convection in comparison to observe percentages. The model tends to underestimate the percentage of convection for Grell–AS and Grell–FC for all regions. In comparison, MIT–EMAN produces percentages closer to observed values. Grell–AS and Grell–FC underestimate convective percent on average for all regions by 20% and 23%, respectively. MIT–EMAN underestimates convective percentage for all regions by only 3%. These results demonstrate that, for the GHA region, the MIT–EMAN convective scheme performs better in the partitioning of stratiform and convective rainfall.

The vertical profile of average θ_e is shown in Fig. 8. The center line in each plot corresponds to the average vertical profile while the other lines are plus or minus one standard deviation from the mean. The average values give a good sense of the typical convective environment for each scheme. Grell–FC has the most stable average profile of the three schemes, with MIT–EMAN

being the least stable. The standard deviations show the spread of θ_e values for which convection can occur. In all schemes the standard deviations are small near the surface, but in both Grell–AS and Grell–FC the spread is large aloft. The larger spread aloft favors both deep and shallow convection. In comparison, MIT–EMAN shows a small spread throughout the vertical domain, and favors deep convection. The production of shallow convection, as shown in the Grell–AS and Grell–FC profiles, may partly explain the negative convective bias over land exhibited in both these schemes. In addition the lack of a shallow convection signal in the MIT–EMAN profile may contribute to the positive convective rainfall bias.

For this domain and season, we found that MIT–EMAN outperforms both Grell–AS and Grell–FC in several areas. The first is the spatial extent of convection, especially over the Congo where little to no rainfall was generated in Grell–AS or Grell–FC. Also, MIT–EMAN generates more rainfall over land than ocean, which is a feature we saw in observations. Finally, MIT–EMAN correctly partitions the stratiform/convective rainfall. The correct partitioning and a consistent positive rainfall bias allows for the possibility of a systematic correction of the rainfall.

c. *SUBEX results*

As shown in the previous section, each convective scheme has its advantages and disadvantages, but for this study MIT–EMAN provides the best results. While MIT–EMAN performs well for the majority of the region, there are several areas, notably eastern Congo, southwestern Ethiopia, and the central to western southern Indian Ocean, where the scheme shows poor agreement with TRMM total rainfall (Fig. 9). Areas within these regions also exhibit the largest disagreement between the model and TRMM convective percentages (Fig. 10). In the model, convective percentages of less than 50% are common in these regions. Some localized areas show convective percentages below 25%. In TRMM, the convective percentage for those regions is above 75% except for a few localized areas above 50%.

1) RH_{min} SENSITIVITY

The next set of experiments was motivated by the fact that qualitative arguments could be made for reducing intense stratiform events by either increasing or decreasing RH_{min}. The relationship of RH_{min} to cloud fraction at varying relative humidities is shown in Fig. 11. The first test was to increase the value of RH_{min} over land from 80% to 90% (RHmin-90). By setting a higher relative humidity threshold, and thereby reducing cloud cover at lower RH values, we presumed that there would be fewer large-scale rain events, reducing the amount of stratiform rainfall. The second sensitivity test lowered the RH_{min} to 60% over both the land and the ocean (RHmin-60). This value increases clouds at lower RH values allowing us to test if more frequent rainfall would prevent excess moisture from being transported to the upper atmosphere before being rained out. Intuitively, for 60% RH_{min}, a 90% gridbox humidity would produce a 30% cloud fraction, potentially allowing rain to occur sooner, preventing the buildup of upper-level moisture and intense stratiform rainfall.

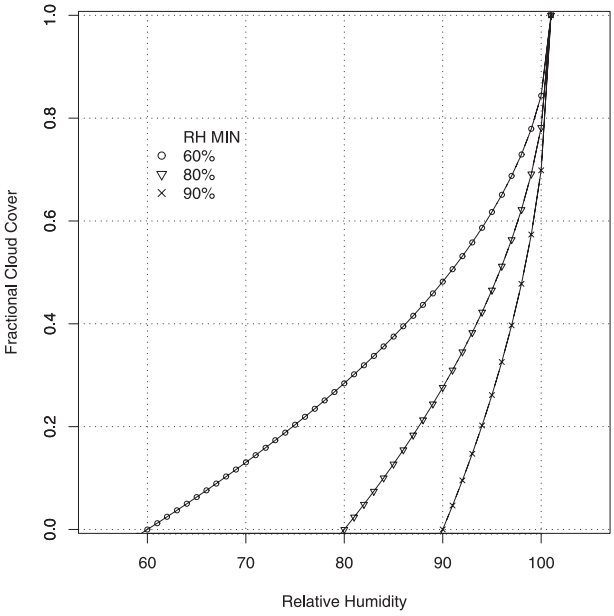

FIG. 11. Relative humidity vs fractional cloud cover for RH_{min} equal to 60% (circles), 80% (triangles), and 90% (crosses).

To quantitatively compare the results shown in Fig. 5, we calculated average percent change between the sensitivity runs and the MIT–EMAN control run for four of the five regions, excluding the SUD region. The SUD region was excluded because of the small rainfall totals over this region that skew the percentage change. We found that the total rain increased marginally, 6.6% on average in the RHmin-90, but decreased significantly, 15.6% on average, in RHmin-60. Since MIT–EMAN has a positive total rainfall bias, it is clear that the RHmin-60 provides an improvement in total rainfall for our domain. However, we found that for RHmin-60 there were increased regions of convective percentage below 50% (Figs. 10a,c). This signifies that the reduction in total precipitation does not come just from the large-scale scheme, as expected, but is also the result of a large reduction in convective rainfall.

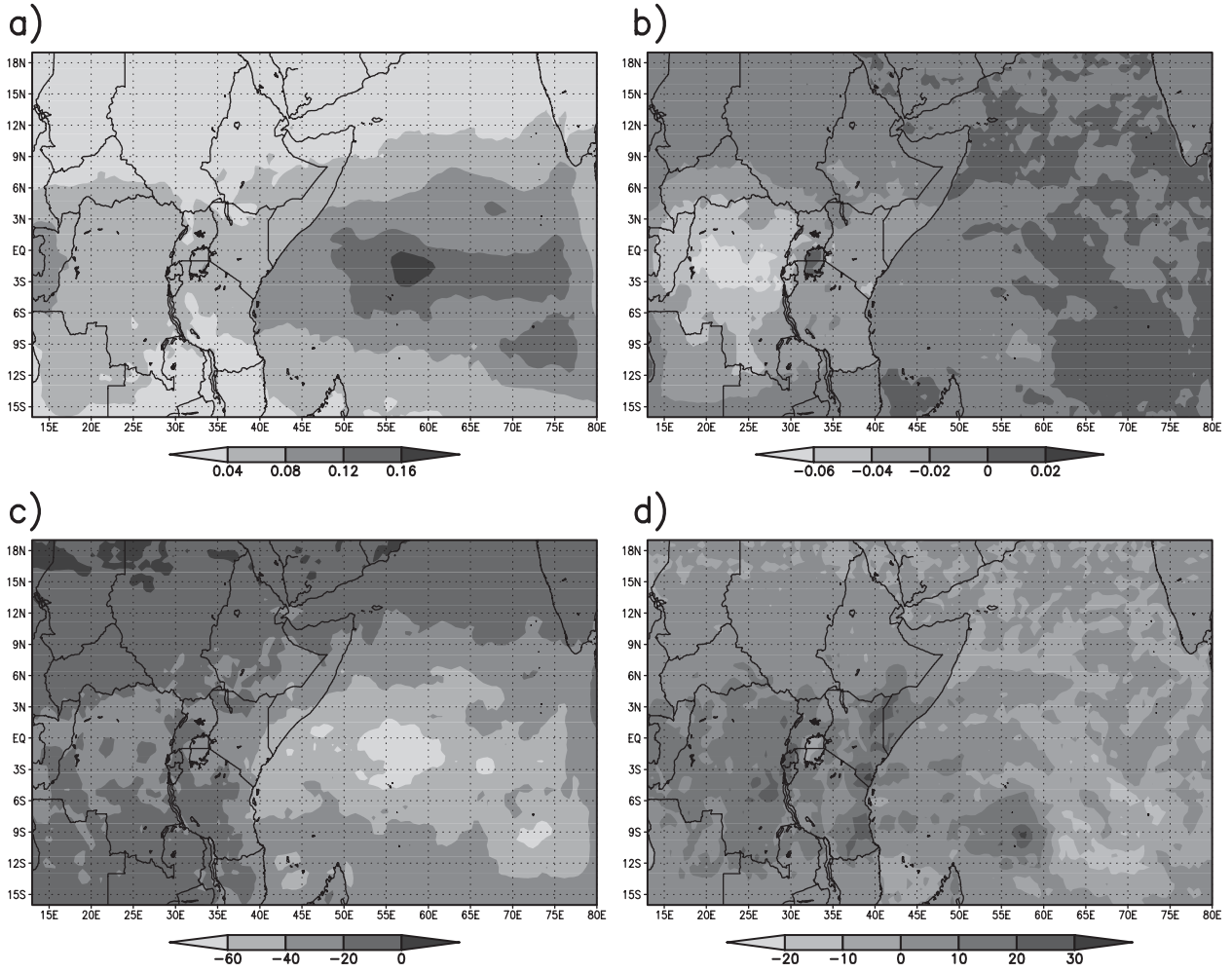

FIG. 12. Cloud fraction difference between (a) RHmin-60 and (b) RHmin-90 and MIT–EMAN. Surface absorbed solar flux (W m^{-2}) difference between (c) RHmin-60 and (d) RHmin-90 and MIT–EMAN.

When the percent change of the convective and stratiform partitions of rainfall are calculated as total rain was above, it can be seen that both RHmin-90 and RHmin-60 affected the convective rainfall more than the stratiform. Both were changed in the same direction (sign) for each test. RHmin-90 shows a 0.3% increase in stratiform rainfall, while there is a 9.1% increase in convective rainfall. In RHmin-60, the convective rainfall is reduced 19.8% compared to only a 3.9% reduction in stratiform. The next step is to determine why changing the fractional cloud cover in the SUBEX scheme would affect convective rainfall more than stratiform. The reason appears to be in the feedback of cloudiness on the thermodynamics of the model.

The convection scheme requires instability to generate rainfall. In the tropics, this instability is caused by solar insolation both heating the surface and evaporating water, thereby moistening the surface. By lowering the grid-average relative humidity requirement for cloud formation, the amount of insolation reaching the surface is reduced because the increased cloud cover reflects more solar energy. This is shown in Fig. 12, where column average cloud cover is calculated from sigma 0.93 to 0.05 and is compared with the surface absorbed solar energy flux. The reduced insolation, displayed in RHmin-60, limits the instability in the atmosphere and thereby reduces the amount of convective precipitation. The opposite occurs in RHmin-90 where clouds are reduced over the GHA especially over the Congo tropical rain forest. This reduction in cloudiness increases the amount of solar radiation that reaches the surface and leads to increased convection.

In addition to reducing insolation, the production of clouds at a lower relative humidity affects the strength

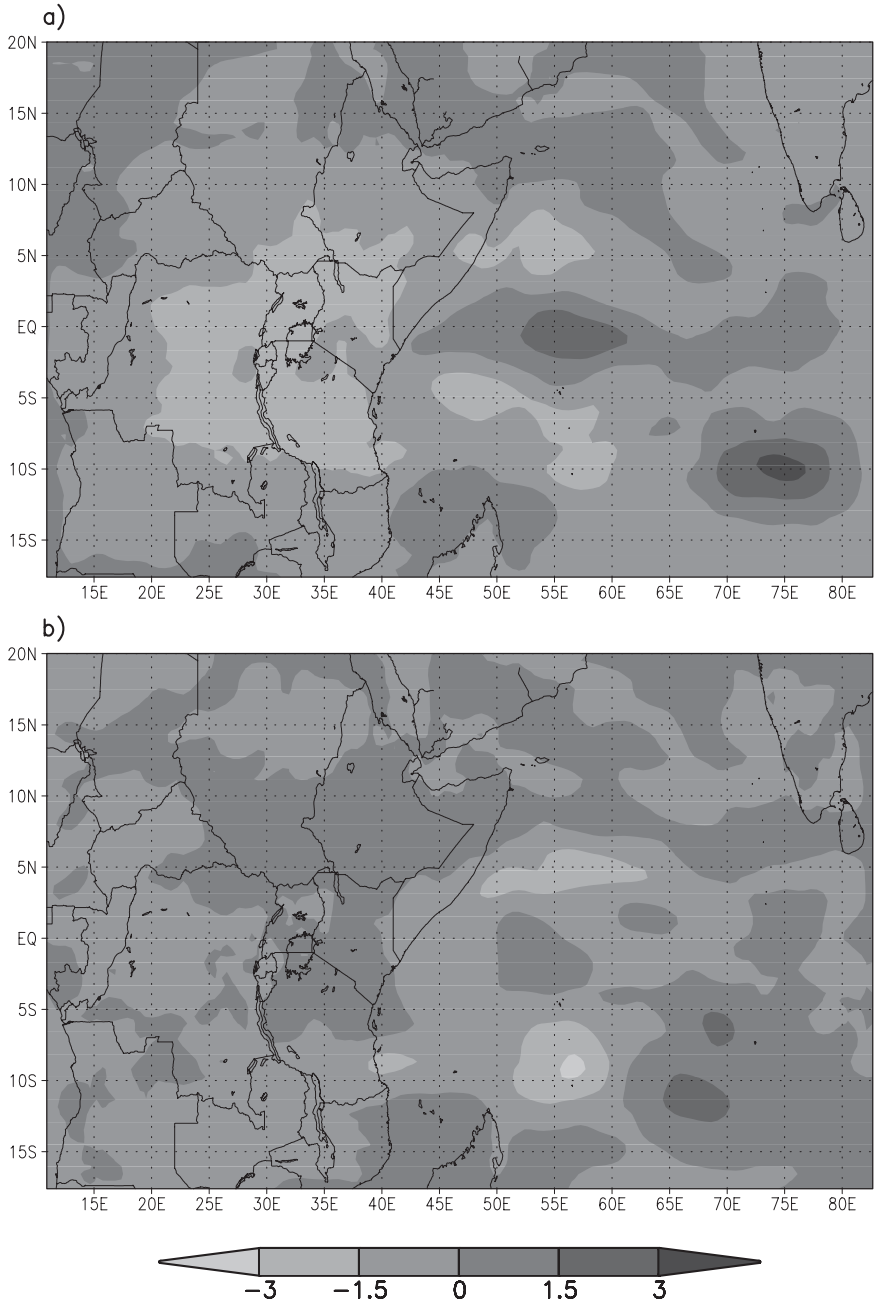

FIG. 13. Vertically averaged moisture difference (kg kg^{-1}) $\times$ 10^{-4} from σ 0.945 to 0.13 for (a) RHmin-60 − MIT–EMAN and (b) RHmin-90 − MIT–EMAN.

and duration of convection after it starts by allowing the atmosphere to stabilize more rapidly. Once convection in the model begins, moisture is transported aloft. This moisture is rained out by both the convective scheme and the SUBEX scheme. In the SUBEX scheme, once a level reaches RH_{min} condensation begins, allowing for precipitation. Therefore, in RHmin-60, condensation begins at an earlier stage of convection. The larger latent heat release at lower relative humidities could cause the atmosphere to stabilize more rapidly. Once the atmosphere is stabilized, the convection stops. Once the convection stops, moisture is no longer transported aloft, reducing rainfall from both schemes. Figure 13 shows the specific humidity difference in the middle of the atmosphere (σ 0.945–0.13). This plot shows that there is less moisture in this level in RHmin-60. The

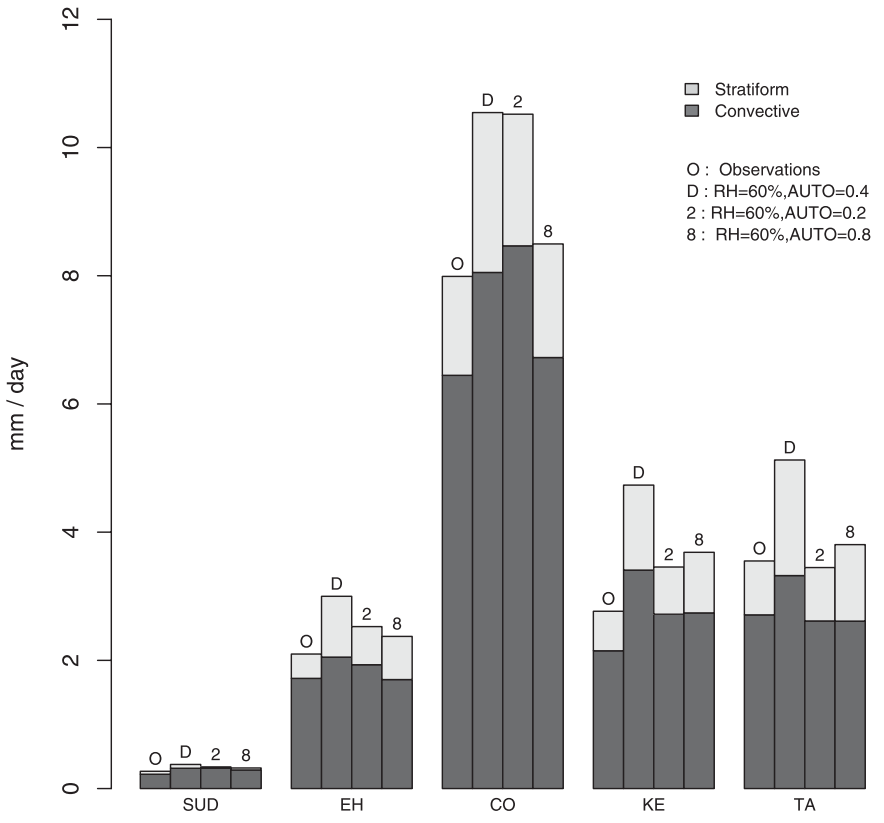

FIG. 14. As in Fig. 5, but for autoconversion scale factor sensitivity tests.

reduced moisture aloft could be caused by two mechanisms. The first is the shorter convection time, which would reduce the amount of moisture transported aloft. The second cause could be a feedback of the weakening of the Congo rain forest convection. In section 5a we noted that the convective circulation in MIT–EMAN was too strong and led to too much moisture being transported from the Atlantic Ocean. With a weakening of convection over the Congo region, this transport would be reduced. While a reduction of moisture aloft would reduce rainfall from both schemes, the model calls the convection scheme first, thereby reducing convective rainfall totals by a larger amount than stratiform rainfall. Based on these sensitivity experiments it is clear that, while reducing the RHmin parameter in SUBEX reduces rainfall, it does not limit the excessive stratiform rainfall.

2) AUTOCONVERSION SCALE FACTOR SENSITIVITY

While RHmin-60 tests showed improvements in total rainfall it did not significantly reduce the stratiform rainfall amounts. Therefore, we chose to perform the autoconversion scale factor sensitivity tests in an effort to further reduce the stratiform rainfall. All of these tests utilized the best model setup, which incorporated the MIT–EMAN convective scheme and an RH_{min} of 60%.

We first started comparing the autoconversion sensitivity using the area-average box method performed in the previous sensitivity tests (Fig. 14). The total amount of rainfall decreases, approaching observations, for both the doubling (C_{acs}-double) and halving (C_{acs}-half) of C_{acs} for all regions. The performance of each sensitivity varies from region to region, but calculation of percent convective rainfall is closer to observations for C_{acs}-half in all regions when excluding the drier SUD region. However, we note that there is a larger decrease over the Congo for C_{acs}-double, thereby more closely matching the observations.

Our next step was to qualitatively compare the sensitivity tests (Fig. 15). Both sensitivity tests decrease the amount of precipitation over the eastern portions of the Greater Horn of Africa, particularly parts of Kenya and Tanzania. The decrease in total precipitation is also notable over the eastern Congo where the maximum amount of precipitation was found in RHmin-60. Over the oceans we again notice a decrease in the total precipitation with the halving sensitivity more realistically capturing the spatial distribution shown in the TRMM observations.

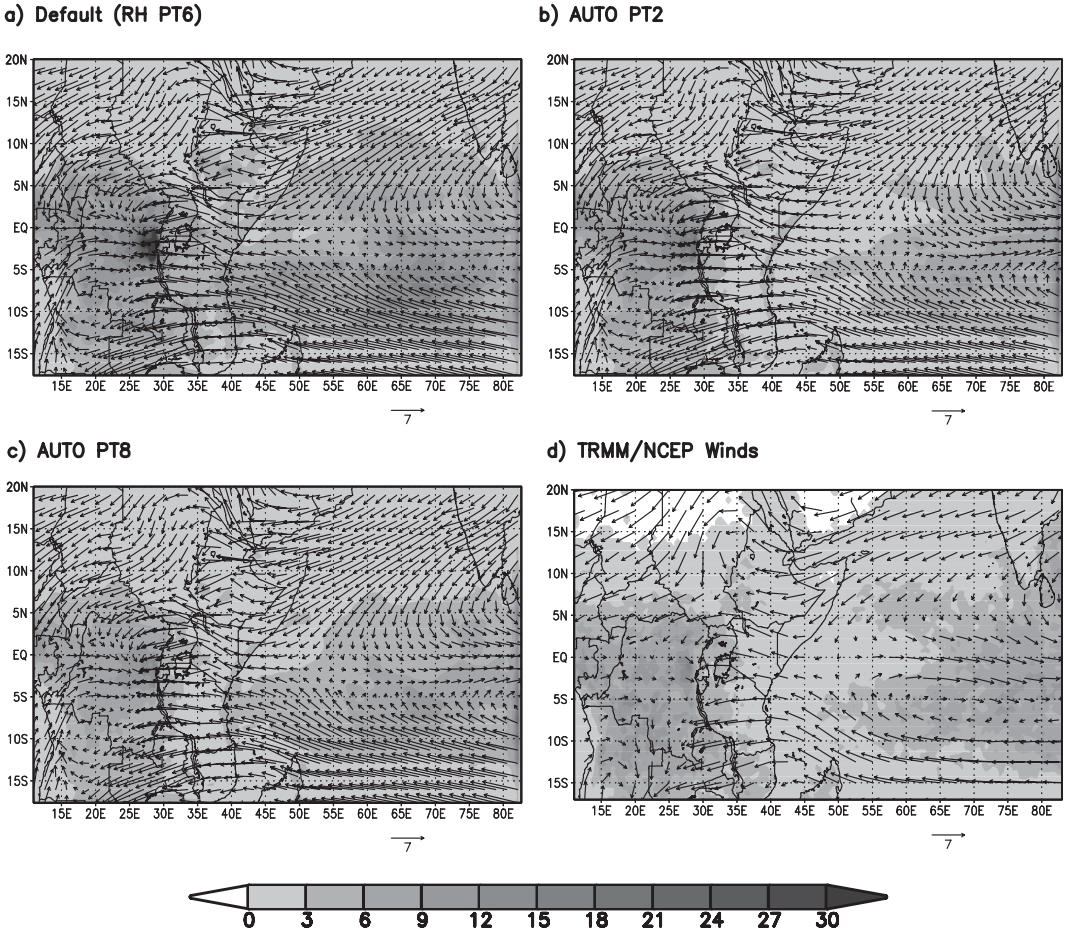

FIG. 15. Three-yr climatological OND rainfall (mm day^{-1}) and 850-mb circulation (m s^{-1}) for autoconversion scale factor sensitivity tests compared with TRMM and NCEP reanalysis winds.

We did not find either C_{acs}-double or C_{acs}-half to clearly outperform the other in terms of rainfall for our region. To better select the optimal autoconversion threshold, we examined the temperature bias for each year of the simulation across all regions (Fig. 16). The temperature bias is smallest for C_{acs}-half for each year and all regions, excluding SUD in 2002. In contrast the temperature bias for the C_{acs}-double is larger than the default in all years and across all regions when excluding SUD for 2002. To determine the reason for these temperature bias results we looked at incoming solar radiation and outgoing longwave cooling for each of the sensitivity tests (not shown). We found that C_{acs}-half had more incoming solar radiation, as well as more outgoing longwave radiation relative to C_{acs}-double; however, the difference in incoming solar was much larger, leading to warming and therefore decreasing the model cold bias. This can be explained by a decrease (increase) in cloudiness for C_{acs}-half (C_{acs}-double) owing to an ability to hold less (more) cloud liquid water aloft before converting it to rain. Additionally, we looked at the timing of rainfall over land and found that more rainfall occurs during the day than at night, which would enhance the effect of this feedback on the incoming solar partition of the energy budget. Based upon the improved spatial distribution, rainfall totals, and temperature, we feel that C_{acs}-half outperforms all other sensitivity tests for our domain.

6. Conclusions and future work

We have examined the moist processes of the RegCM3 regional climate model for an African–Indian Ocean domain. We compared two convective schemes, Grell with closures AS and FC and MIT–EMAN, with TRMM satellite rainfall rates focusing on the amount and partitioning of convective and stratiform precipitation. After determining the best convective scheme for the region, the parameters RH_{min} and C_{acs} in the

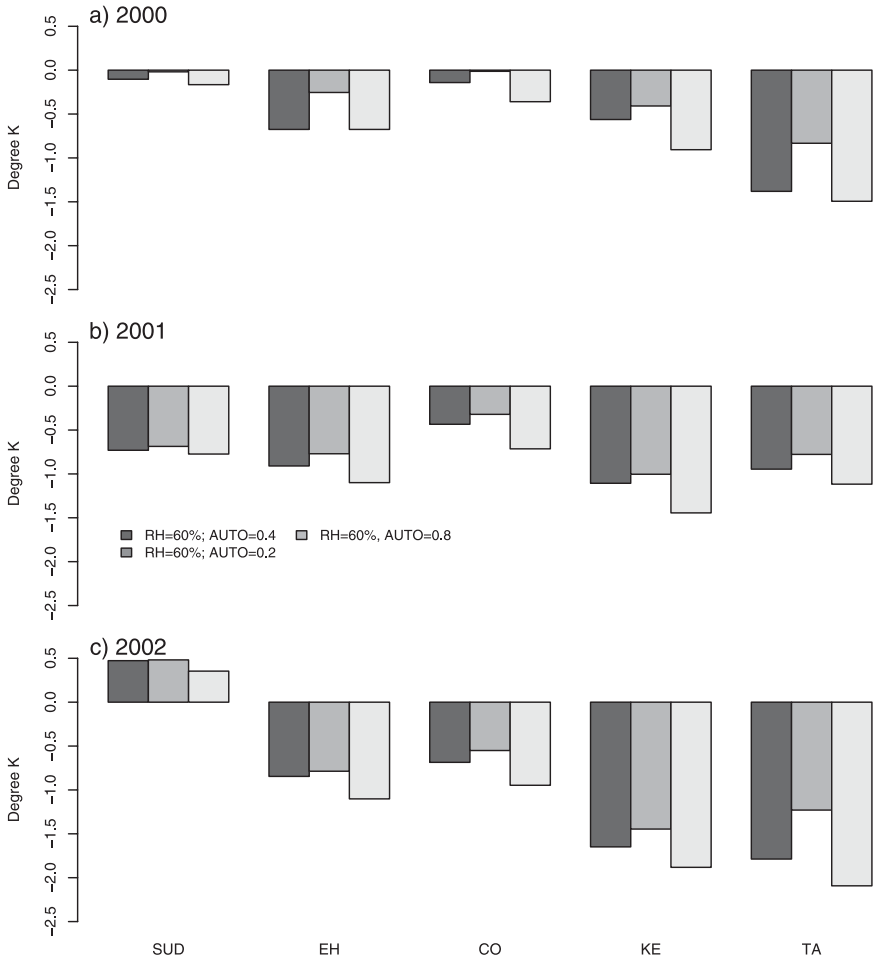

FIG. 16. Yearly OND temperature bias using CRU observations of autoconversion scale factor sensitivity tests for each of the 3 yr in our study across the five heterogeneous rainfall regions.

SUBEX large-scale precipitation scheme were adjusted to provide sensitivity analysis in a tropical environment. The experiments explored qualitative and quantitative comparisons against observations to provide a better understanding of modeled rainfall over the GHA.

The comparison of convective schemes found MIT–EMAN to be the best scheme for our region, based on the criteria examined in this study. It not only provided a more realistic partitioning of convective and stratiform rainfall, but also produced large convective rainfall rates over the GHA, at levels comparable to the TRMM observations. While MIT–EMAN had a large positive total rainfall bias, the consistency of this bias and the realistic rainfall partitioning could enable future studies to further improve the total rainfall rates. Such improvements could include using the MIT–EMAN scheme with convection suppression criteria, which has been found useful in improving RCM performance in simulating the Asian summer monsoon precipitation (Chow et al. 2006). In addition, the smaller biases provided by both Grell–AS and Grell–FC are often the result of an underprediction of convective rainfall coupled with the systematic overprediction of stratiform rain in RegCM3.

Rather unexpectedly, the adjustment of RH_{min} provided a large impact on convective rainfall rates, with a decrease in RH_{min} to 60% (RHmin-60) providing 19.8% less convective rainfall. This is counterintuitive to initial thought, that adjusting parameters in SUBEX would affect stratiform rain more than the convective form. When using the MIT–EMAN scheme, the convective rainfall rates in the model seem to be highly sensitive to the cloud cover. Since RH_{min} directly affects model cloudiness, it appears that this parameter could enable the reduction of the positive convective bias in the MIT–EMAN scheme. Unfortunately, the sensitivity tests of RH_{min} did not provide a significant reduction in stratiform rain rates.

The halving of the of autoconversion scale factor (C_{acs}-half) provided an improvement in the spatial distribution of rainfall and the temperature bias. C_{acs}-half also decreased the overprediction of rainfall by the SUBEX scheme, and reduced rainfall totals closer to observed values. Out of all simulations tested in this study, we found the MIT–EMAN convective scheme combined with SUBEX adjustable parameters of RH_{min} of 60% and a value of 0.2, halving the default, for C_{acs} worked best for our domain over the time period studied.

Future work will focus on further reducing the stratiform rain rates provided by the SUBEX scheme in a tropical environment. The autoconversion of cloud water to rainwater is one area that may provide this reduction. The current autoconversion calculation in the model relies on a relationship between temperature and LWC that was derived for mid–high latitudes. This calculation needs to be either updated or replaced for the tropics, as tropical LWC has been shown to exceed the values used to derive the current relationship (Gultepe and Isaac 1997; Iacobellis and Somerville 2000). We did not attempt to find a formulation for LWC in the tropics, which would require identifying the necessary data for our region to derive a new formulation for autoconversion. However, development of a more suitable algorithm for this region should be a matter of high priority and we reserve it for future studies. Additionally, the future Global Precipitation Measuring Mission will provide improved measurements of both rainfall and cloud properties, allowing for further improvement of moist processes in regional climate models.

Acknowledgments. This research was supported by NSF Climate Dynamics Program 0438116. We would like to acknowledge the high performance computing center at North Carolina State University for providing the computational platform used to perform the RegCM3 model simulations. The postprocessing of the data was in part computed in the NCSU Climate Modeling Lab. Some of these calculations would not have been possible without the R open source statistical package available at http://cran.r-project.org.

The data used in this study were acquired as part of the Tropical Rainfall Measuring Mission (TRMM). The algorithms were developed by the TRMM Science Team. The data were processed by the TRMM Science Data and Information System (TSDIS) and the TRMM Office; they are archived and distributed by the Goddard Distributed Active Archive Center. TRMM is an international project jointly sponsored by the Japan National Space Development Agency (NASDA) and the U.S. National Aeronautics and Space Administration (NASA) Office of Earth Sciences.

REFERENCES

Anthes, R., 1977: A cumulus parameterization scheme utilizing a one-dimensional cloud model. *Mon. Wea. Rev.,* **105,** 270–286.

Anyah, R. O., and F. H. M. Semazzi, 2007: Variability of East African rainfall based on multiyear RegCM3 simulations. *Int. J. Climatol.,* **27,** 357–371.

——, ——, and L. Xie, 2006: Simulated physical mechanisms associated with multiscale climate variability over Lake Victoria Basin in East Africa. *Mon. Wea. Rev.,* **134,** 3588–3609.

Arakawa, A., and W. H. Schubert, 1974: Interaction of a cumulus cloud ensemble with the large-scale environment, Part I. *J. Atmos. Sci.,* **31,** 674–701.

Behera, S. K., J.-J. Luo, S. Masson, P. Delecluse, S. Gualdi, A. Navarra, and T. Yamagata, 2005: Paramount impact of the Indian Ocean dipole on the East African short rains: A CGCM study. *J. Climate,* **18,** 4514–4530.

Black, E., J. Slingo, and K. R. Sperber, 2003: An observational study of the relationship between excessively strong short rains in coastal East Africa and Indian SST. *Mon. Wea. Rev.,* **131,** 74–94.

Bowden, J. H., 2004: Recent and projected climate variability during the seasonal rains of the Greater Horn of Africa. M.S. thesis, Marine, Earth, and Atmospheric Science, North Carolina State University, 213 pp.

Chow, K. C., J. C. L. Chan, J. S. Pal, and F. Giorgi, 2006: Convection suppression criteria applied to the MIT cumulus parameterization scheme for simulating the Asian summer monsoon. *Geophys. Res. Lett.,* **33,** L24709, doi:10.1029/2006GL028026.

Cotton, W. R., and R. A. Anthes, 1989: *Storm and Cloud Dynamics*. Academic Press, 883 pp.

Del Genio, A. D., M.-S. Yao, W. Kovari, and K. K.-W. Lo, 1996: A prognostic cloud water parameterization for global climate models. *J. Climate,* **9,** 270–304.

Dickinson, R., A. Henderson-Sellers, and P. Kennedy, 1993: Biosphere–Atmosphere Transfer Scheme (BATS) version 1e as coupled to the near community climate model. Tech. Rep., National Center for Atmospheric Research, 72 pp.

Emanuel, K. A., 1991: A scheme for representing cumulus convection in large-scale models. *J. Atmos. Sci.,* **48,** 2313–2335.

——, and M. Zivkovic-Rothman, 1999: Development and evaluation of a convection scheme for use in climate models. *J. Atmos. Sci.,* **56,** 1766–1782.

Fritsch, J. M., and C. F. Chappell, 1980: Numerical prediction of convectively driven mesoscale pressure systems. Part I: Convective parameterization. *J. Atmos. Sci.,* **37,** 1722–1733.

Giorgi, F., and C. Shields, 1999: Tests of precipitation parameterizations available in latest version of NCAR regional climate model (RegCM) over continental United States. *J. Geophys. Res.,* **104** (D6), 6353–6375.

——, and L. O. Mearns, 1999: Introduction to special section: Regional climate modeling revisited. *J. Geophys. Res.,* **104** (D6), 6335–6352.

——, M. R. Marinucci, and G. T. Bates, 1993a: Development of a second-generation regional climate model (RegCM2). Part I: Boundary-layer and radiative transfer processes. *Mon. Wea. Rev.,* **121,** 2794–2813.

——, ——, ——, and G. DeCanio, 1993b: Development of a second-generation regional climate model (RegCM2). Part II: Convective processes and assimilation of lateral boundary conditions. *Mon. Wea. Rev.,* **121,** 2814–2832.

Grell, G., 1993: Prognostic evaluation of assumptions used by cumulus parameterizations. *Mon. Wea. Rev.,* **121,** 764–787.

Gultepe, I., and G. A. Isaac, 1997: Liquid water content and temperature relationship from aircraft observations and its applicability to GCMs. *J. Climate,* **10,** 446–452.

Holtslag, A., E. de Bruijn, and H.-L. Pan, 1990: A high resolution air mass transformation model for short-range weather forecasting. *Mon. Wea. Rev.,* **118,** 1561–1575.

Houze, R. A., Jr., 1997: Stratiform precipitation in regions of convection: A meteorological paradox? *Bull. Amer. Meteor. Soc.,* **78,** 2179–2196.

Iacobellis, S. F., and R. C. Somerville, 2000: Implications of microphysics for cloud-radiation parameterizations: Lessons from TOGA COARE. *J. Atmos. Sci.,* **57,** 161–183.

Indeje, M., F. H. M. Semazzi, and L. J. Ogallo, 2000: ENSO signals in East African rainfall seasons. *Int. J. Climatol.,* **20,** 19–46.

Ininda, J. M., 1994: Numerical simulation of the influence of the sea surface temperature anomalies on the east African seasonal rainfall. Ph.D. thesis, University of Nairobi, Kenya, 305 pp.

——, 1998: Simulation of the impact of sea surface temperature anomalies on the short rains over East Africa. *J. Afr. Meteor. Soc.,* **3,** 127–138.

Kistler, R., and Coauthors, 2001: The NCEP–NCAR 50-Year Reanalysis: Monthly means CD-ROM and documentation. *Bull. Amer. Meteor. Soc.,* **82,** 247–268.

Kummerow, C., and Coauthors, 2001: The evolution of the Goddard Profiling Algorithm (GPROF) for rainfall estimation from passive microwave sensors. *J. Appl. Meteor.,* **40,** 1801–1820.

Mitchell, T. D., and P. D. Jones, 2005: An improved method of constructing a database of monthly climate observations and associated high-resolution grids. *Int. J. Climatol.,* **25,** 693–712.

Nicholson, S. E., 1996: A review of climate dynamics and climate variability in eastern Africa. *The Limnology, Climatology and Paleoclimatology of the East African Lakes,* T. C. Johnson and E. O. Odada, Eds., Gordon and Breach Publishers, 25–56.

——, J. Kim, and J. Hoopingarner, 1988: *Atlas of African Rainfall and Its Interannual Variability*. Florida State University, 237 pp.

Pal, J. S., E. E. Small, and E. A. B. Eltahir, 2000: Simulation of regional-scale water and energy budgets: Representation of subgrid cloud and precipitation processes within RegCM. *J. Geophys. Res.,* **105** (D24), 29 579–29 594.

——, and Coauthors, 2007: Regional climate modeling for the developing world: The ICTP RegCM3 and RegCNET. *Bull. Amer. Meteor. Soc.,* **88,** 1395–1409.

Reynolds, R. W., and T. M. Smith, 1994: Improved global sea surface temperature analyses using optimum interpolation. *J. Climate,* **7,** 929–948.

Robertson, F. R., D. E. Fitzjarrald, and C. D. Kummerow, 2003: Effects of uncertainty in TRMM precipitation radar path integrated attenuation on interannual variations of tropical oceanic rainfall. *Geophys. Res. Lett.,* **30,** 1180, doi:10.1029/2002GL016416.

Schumacher, C., and R. A. Houze Jr., 2003: Stratiform rain in the tropics as seen by the TRMM precipitation radar. *J. Climate,* **16,** 1739–1755.

Sun, L.-Q., F. Semazzi, F. Giorgi, and L. Ogallo, 1999a: Application of the NCAR regional climate model to eastern Africa, 1. Simulation of the short rains of 1988. *J. Geophys. Res.,* **104,** 6529–6548.

——, ——, ——, and ——, 1999b: Application of the NCAR regional climate model to eastern Africa, 2. Simulation of interannual variability of short rains. *J. Geophys. Res.,* **104,** 6549–6562.

Sundqvist, H., 1988: Parameterization of condensation and associated clouds in models for weather prediction and general circulation simulation. *Physically-Based Modelling and Simulation of Climate and Climactic Change,* Part 1, M. E. Schlesinger, Ed., Kluwer Academic Publishers, 433–461.

Vaidya, S. S., 2006: The performance of two convective parameterization schemes in a mesoscale model over the Indian region. *Meteor. Atmos. Phys.,* **92** (3–4), 175–190.

Wang, Y., L. R. Leung, J. L. McGregor, D.-K. Lee, W.-C. Wang, Y. Ding, and F. Kimura, 2004: Regional climate modeling: Progress, challenges and prospects. *J. Meteor. Soc. Japan,* **82,** 1599–1628.

Zhao, Q., T. L. Black, and M. E. Baldwin, 1997: Implementation of the cloud prediction scheme in the Eta model at NCEP. *Wea. Forecasting,* **12,** 697–712.